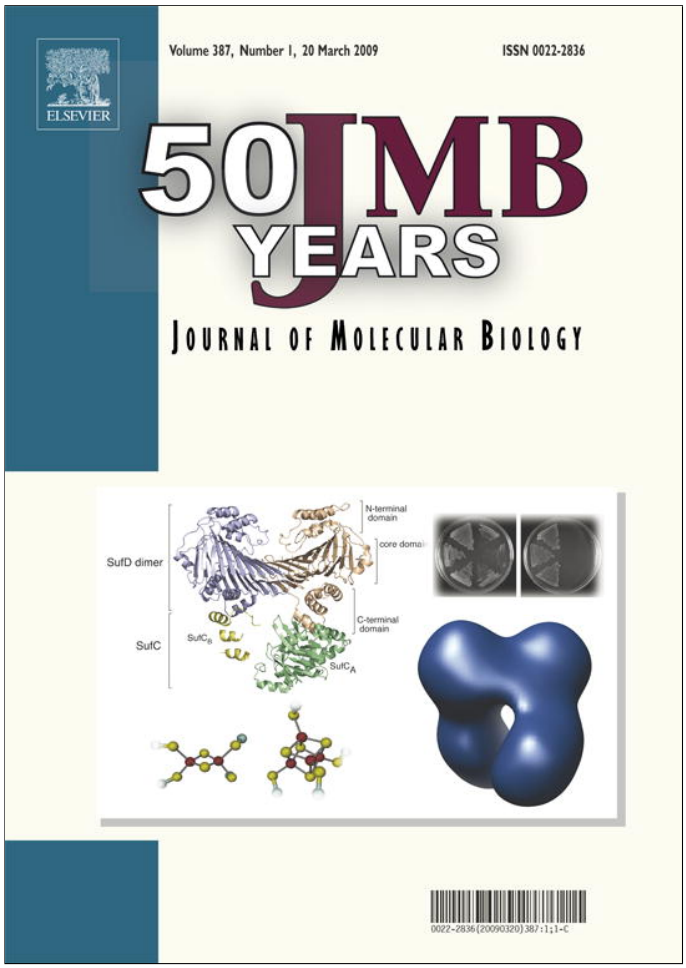

doi:10.1016/j.jmb.2009.01.030 J. Mol. Biol. (2009) 387, 175–191

JMB

Available online at www.sciencedirect.com

ScienceDirect

ELSEVIER

Pentameric Assembly of Potassium Channel Tetramerization Domain-Containing Protein 5

Irina S. Dementieva[1]†, Valentina Tereshko[2]†, Zoe A. McCrossan[1], Elena Solomaha[2], Daniel Araki[1], Chen Xu[3], Nikolaus Grigorieff[3,4] and Steve A. N. Goldstein[1]*

[1]*Department of Pediatrics and Institute of Molecular Pediatric Sciences, University of Chicago, Chicago, IL 60637, USA*

[2]*Department of Biochemistry and Molecular Biology, University of Chicago, Chicago, IL 60637, USA*

[3]*Rosenstiel Basic Medical Sciences Research Center, Waltham, MA 02454, USA*

[4]*Howard Hughes Medical Institute, Brandeis University, Waltham, MA 02454, USA*

Received 5 September 2008; received in revised form 16 January 2009; accepted 19 January 2009
Available online 23 January 2009

Edited by J. Bowie

We report the X-ray crystal structure of human potassium channel tetramerization domain-containing protein 5 (KCTD5), the first member of the family to be so characterized. Four findings were unexpected. First, the structure reveals assemblies of five subunits while tetramers were anticipated; pentameric stoichiometry is observed also in solution by scanning transmission electron microscopy mass analysis and analytical ultracentrifugation. Second, the same BTB (*b*ric-a-brac, *t*ramtrack, *b*road complex) domain surface mediates the assembly of five KCTD5 and four voltage-gated K^+ (Kv) channel subunits; four amino acid differences appear crucial. Third, KCTD5 complexes have well-defined N- and C-terminal modules separated by a flexible linker that swivels by ~30°; the C-module shows a new fold and is required to bind Golgi reassembly stacking protein 55 with ~1 μM affinity, as judged by surface plasmon resonance and ultracentrifugation. Fourth, despite the homology reflected in its name, KCTD5 does not impact the operation of Kv4.2, Kv3.4, Kv2.1, or Kv1.2 channels.

Keywords: KCTD5; BTB; Kv channel; T1 domain; GRASP55

Introduction

The human genome has 21 *KCTD* genes that encode potassium channel tetramerization domain-containing (KCTD) proteins. *KCTD* genes are so named because the N-termini of KCTD proteins and some voltage-gated K^+ (Kv) channels are homologous.[1,2] Four Kv channel subunits aggregate to create a transmembrane ion conduction pathway; subunit assembly is expedited by N-terminal tetramerization (T1) domains that contain a BTB (*b*ric-a-brac, *t*ramtrack, *b*road complex) fold.[3,4] KCTD proteins are soluble with N-terminal BTB domains and variable C-termini.[5] Because Kv channels operate in tissue-specific fashion due to interaction with accessory subunits that modify subcellular location, level of expression, activity, and pharmacology,[6] KCTDs had been anticipated to bind to and regulate Kv channels.

Originally identified in *Drosophila melanogaster* zinc finger proteins, BTB (also called Poxvirus zinc finger) motifs are protein–protein interaction modules that mediate both self-association and interaction with non-BTB partners. Structures of proteins with BTB domains show significant conservation of the core

*Corresponding author. E-mail address: sangoldstein@uchicago.edu.

† I.S.D. and V.T. contributed equally to this work.

Abbreviations used: KCTD5, potassium channel tetramerization domain-containing protein 5; Kv, voltage-gated K^+; KCTD, potassium channel tetramerization domain-containing protein; GRASP55, Golgi reassembly stacking protein 55; SAD, single-wavelength anomalous dispersion; PDB, Protein Data Bank; STEM, scanning transmission electron microscopy; SV, sedimentation velocity; SE, sedimentation equilibrium; HEK293, human embryonic kidney cell line 293T; SPR, surface plasmon resonance; KChIP2, Kv channel interacting protein 2; CHO, Chinese hamster ovary; HA, hemagglutinin A.

Table 1. Data collection and refinement statistics for KCTD5 crystals

	Selenomethionine-labeled high-salt KCTD5 (PDB ID 3DRX)	Native low-salt KCTD5 (PDB ID 3DRY)	N-terminal domain (PDB ID 3DRZ)
Data collection			
Space group	$P2_12_12_1$	$P2_12_12_1$	$P2_12_12_1$
Cell dimensions			
a, *b*, *c* (Å)	72.9, 128.6, 152.5	103.0, 106.8, 110.1	59.03, 90.72, 110.16
α, β, γ (°)	90, 90, 90	90, 90, 90	90, 90, 90
Resolution (Å)[a]	20–3.1 (3.2–3.1)	20–3.3 (3.4–3.3)	20–1.9 (1.95–1.90)
R_{merge}[a]	0.072 (0.46)	0.089(0.56)	0.065 (0.45)
I/σ[a]	12.4 (2.3)	11.3 (2.0)	15.4 (2.5)
Completeness (%)[a]	98.9 (93.8)	99.7 (98.5)	99.7 (98.4)
Redundancy[a]	4.4 (4.5)	4.3 (4.4)	4.5 (4.5)
Refinement			
Resolution (Å)	20–3.1	20–3.3	20–1.9
Number of reflections	25,986	18,687	46,924
R_{work}/R_{free}	0.227/0.275	0.252/0.308	0.193/0.232
Number of atoms			
Protein	6915	6815	4095
Water	—	—	359
B-factors			
Protein	67	73	35.1
Water	—	—	42.0
RMSD			
Bond lengths (Å)	0.008	0.012	0.009
Bond angles (°)	1.05	1.28	1.196

One crystal was used for each data collection.
[a] Data in parentheses correspond to the last resolution shell.

fold; the domains are known to mediate the homodimeric and homotetrameric assembly of transcription factors and Kv channels, respectively, using different surfaces of the fold.[7]

The biological function of KCTD proteins remains unclear. Robust expression of transcripts in fetal tissues and low levels in adults suggest that they play a role during development.[8] Thus, KCTD12 (pfetin/Ron) is implicated in the maturation of inner ear neurons by linkage to a progressive dominant auditory neuropathy,[9] and KCTD11 is proposed to suppress Hedgehog signaling and to promote tumor growth in medulloblastoma.[10,11] A point mutation in KCTD7 has been associated with neurodegeneration and progressive myoclonic epilepsy,[12] and potassium channel tetramerization domain-containing protein 5 (KCTD5) has been reported to interact with human Golgi reassembly stacking protein 55 (GRASP55).[13]

We studied human KCTD5 because it had both the highest predicted solubility and a strong level of homology to Kv channels among KCTD proteins. X-ray single-wavelength anomalous dispersion (SAD) technique was used to determine the structure at 3.1 and 3.3 Å resolution after crystallization in two salt conditions; the N-terminal BTB-containing module was solved on its own at 1.9 Å. It is rare but known for a domain to produce several oligomerization states using the same protein–protein interface.[14] Unexpectedly, KCTD5 reveals how four substitutions in a BTB domain permit the same interface to bring together five KCTD5 subunits rather than four Kv channel T1 domains.

Results

KCTD5 crystallizes in pentameric assemblies

Human KCTD5 from residue 34 to the C-terminus (201 residues) was expressed in bacteria. Native and selenomethionine-labeled proteins were purified to homogeneity and crystallized. Two orthorhombic $P2_12_12_1$ crystal forms (Table 1) were obtained—one in high-salt conditions and the other in low-salt conditions (Methods). The structure was solved by SAD technique at 3.1 Å resolution, with selenomethionine-labeled protein crystals grown in high salt. The low-salt structure was solved by molecular replacement at 3.3 Å using native crystals. Surprisingly, the structure revealed KCTD5 to be pentameric (Fig. 1a–d) rather than tetrameric like Kv channels.[1,2]

To assess the physical basis for KCTD5 pentamerization, the C-terminal domain was deleted and the N-terminal BTB domain was crystallized alone (Methods). This structure was determined from orthorhombic $P2_12_12_1$ crystals at 1.9 Å resolution by molecular replacement; again, a pentameric organization was revealed (Table 1). The structure of an individual KCTD5 subunit is shown in Fig. 2. Alignment of KCTD5 sequence and secondary structure are shown in Fig. 3. The KCTDs can be sorted into six groups and KCTD20 based on the homology of their N-termini (Fig. 3). Residues 44–211 form the core of the assembly, forming six α-helices (α1–α6) and six β-strands (β1–β6). The N-terminal residues 44–149 adopt a familiar BTB fold

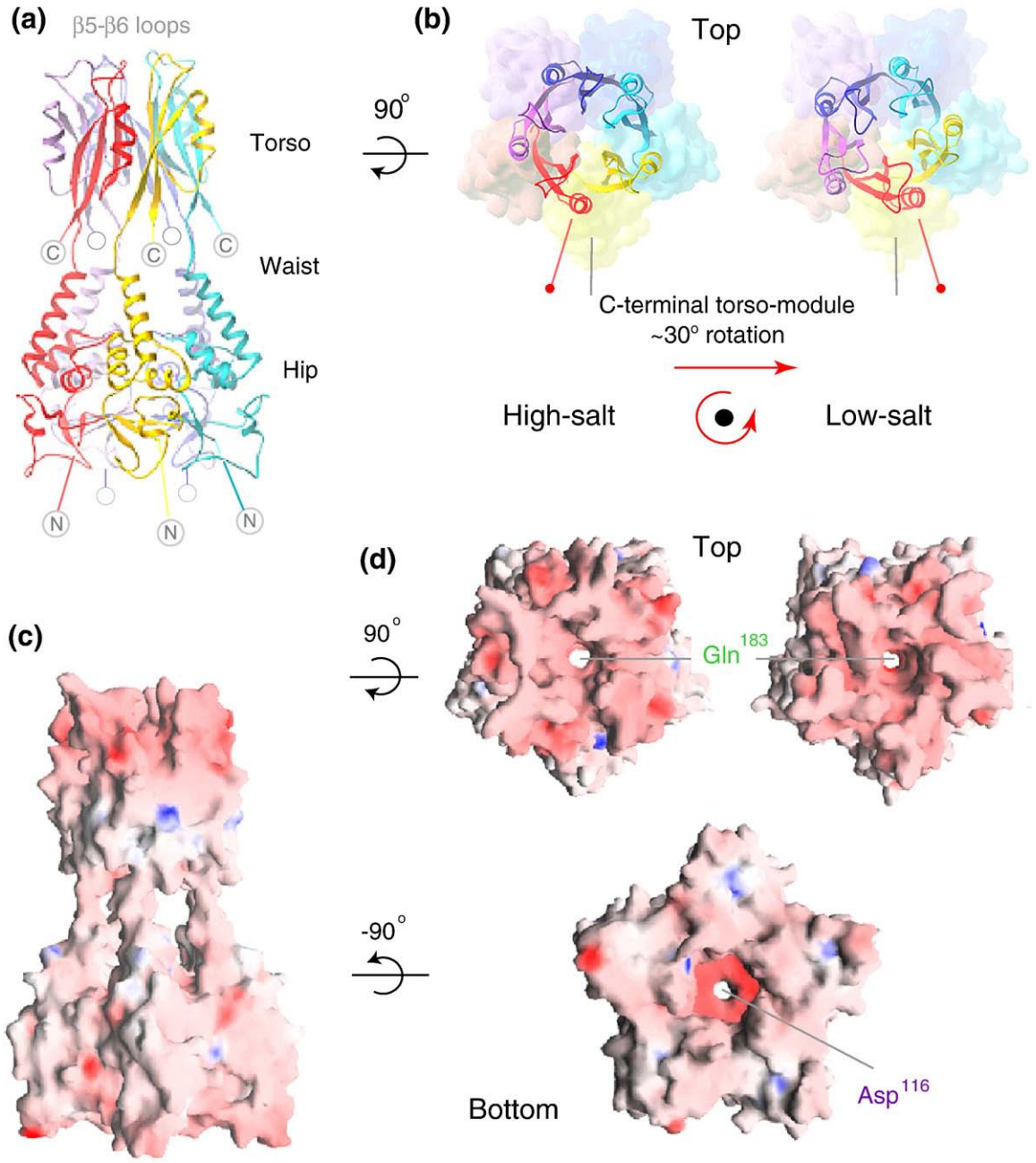

Fig. 1. Architecture of KCTD5 by X-ray crystallography. (a) Side-view ribbon representation of KCTD5 complexes (residues 44–211; high-salt crystal form); the five subunits are in red, yellow, cyan, blue, and violet. The N-module (hip), interdomain linker (waist), C-module (torso), and β5–β6 loops are labeled. N-terminal amino acids 1–33 and C-terminal residues 212–234 are not in the crystal structure and are indicated by gray circles. (b) Orientation of the C-module (residues 155–211; ribbons) relative to the N-module (residues 44–149; molecular surface). Top views for two different crystal forms: high-salt (left) and low-salt (right) crystals. Color scheme as in (a). To highlight the change in orientation, N-modules in high-salt and low-salt crystals are aligned, and α6 is marked. The β5–β6 loops are modeled as in the well-defined electron density maps of the blue (high-salt) or cyan (low-salt) subunits; more details on these loops are presented in Fig. S1. (c) Electrostatic surface representation side view of high-salt crystal form. Blue is electropositive, and red is electronegative. (d) Electrostatic surface representation: top views (upper) for high-salt (left) and low-salt (right) crystal forms aligned via their N-modules, and bottom view (lower) for high-salt crystal form. Color scheme as in (c).

with a three-stranded β-sheet (β1–β3) and five α-helices (α1–α5). Superposition of the KCTD5 BTB domain and Kv4.2 channel T1 domain [Protein Data Bank (PDB) ID 1NN7] shows significant structural conservation with an average root mean square deviation (RMSD) value of ~1.7 Å over 92 C^{α} atoms. Four layers (L1–L4) in the BTB fold are defined as for the Kv channel T1 domain.[15] C-terminal residues 155–211 adopt a novel three-dimensional arrangement with a three-stranded β-sheet (β4–β6) and one α-helix (α6) (Fig. 2; Fig. S1) without a Dali search match.[16]

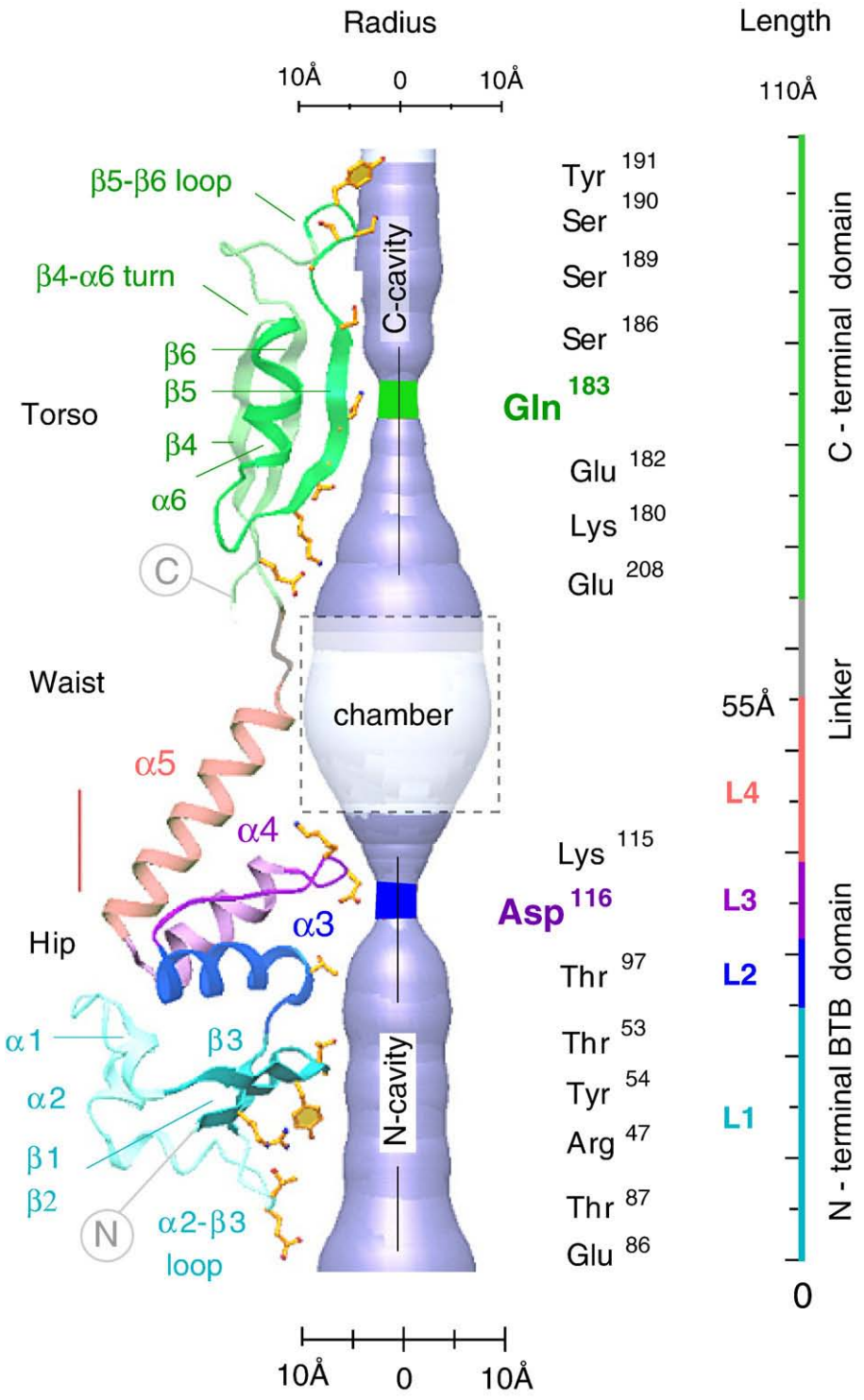

Fig. 2. Structural determinants of the KCTD5 central cavity. A KCTD5 subunit in ribbon presentation showing the four segments (L1–L4) of the BTB fold and the central cavity of the pentamer assembly in cut-away. The residues that shape the central cavity are labeled in ball-and-stick mode; also shown are the solvent-accessible surfaces and cavity dimensions.

While neither is present in the crystal structures, the KCTD5 termini are predicted to be exposed in the cytoplasm. Residues 1–33 were not encoded in the protein because they were predicted to be unstructured by the algorithm of Li *et al.*[17] C-terminal residues 212–234 were not visible on electron density maps. Residues 34–43 adopt different conformations in high-salt and low-salt crystals. Other flexible regions include residues 77–82 near the α2-helix and residues 188–200 near the β5–β6 loops.

Gown-shaped assemblies with two modules

The architecture of KCTD5 complexes (residues 44–211) revealed by X-ray crystallography is shown from the side (Fig. 1a and c) and bottom (Fig. 1d) in high-salt conditions, and from the top (Fig. 1b and d) in both high-salt and low-salt conditions. The five subunits assemble in a circular manner, with N- and C-terminal residues forming distinct N- and C-modules. Views from the top and bottom show each module to be pentameric, with each subunit related by ~72° rotation. The overall assembly is gown-like and ~120 Å tall, with diameters of ~60 Å at the torso, ~40 Å at the waist linker, and ~75 Å at the hips (Figs. 1a and c and 2). The hips are formed by N-terminal residues 44–149 (β-sheets 1–3 and α-helices 1–5, with the N-termini of α3 and α4 facing the center of the assembly). The torso is formed by C-terminal residues 155–211 (β-sheets 4–6 and α-helix 6, with β5 facing the center of the assembly). The interdomain waist (residues 150–154) is flexible and allows a rotation of ~30° between the N-modules and the C-modules; this is demonstrated by a comparison of the crystal forms obtained in high-salt and low-salt conditions (Fig. 1b and d).

Central cavity

The KCTD5 assembly displays a central cavity of variable diameter that is shown from top and bottom (Fig. 1d) and in cut-away (Fig. 2). The cavity appears to be continuous through the 110 Å extent of the central portion of the assembly, 10–15 Å in diameter at its ends, and 20 Å at a windowed chamber, with access to bulk solvent formed by the interdomain linker and α-helices atop the N-module (Fig. 1c). The cavity narrows twice to ~4.5 Å at five Gln183 residues in the C-module and at five Asp116 residues in the N-module. The cavity is lined predominantly by hydrophilic residues (Fig. 2). The C-terminal portion of the cavity is formed by β5-strand residues Glu182, Gln183, Ser186, and Gly188. The N-terminal portion is formed mainly by residues Thr53, Tyr54, Thr97, Lys115, and Asp116 that are scattered across the β2-strand, α3-helix, and tip of the α3–α4 loop. Around 90 well-ordered water molecules are apparent within the N-module portion of the cavity in the 1.9 Å structure. A cation could fit into the assembly at the five Asp116 residues, but the electron density difference map (above 2σ) was not revealing.

KCTD5 is also pentameric in solution

The two modules and five subunits observed in crystallized KCTD5 complexes were observed as well for assemblies studied in solution (Fig. 4). Electron microscopy of individual particles stained with uranyl acetate showed two domains linked by a thin stalk with a long dimension of ~110 Å and a width of ~70 Å (Fig. 4a). Quantitative mass analysis using scanning transmission electron microscopy (STEM) revealed a unimodal distribution with a mean value of 107±16 kDa, in good agreement with the expected mass of KCTD5 (34–234) pentamers (~115 kDa) (Fig. 4b). Sedimentation velocity (SV) studies also gave the expected masses for KCTD5 and N-module pentamers (~115 and ~ 62 kDa, respectively; data not shown). While analytical gel-filtration chromatography suggested a mass about twice that expected (~230 kDa; data not shown), this appeared to be due to confounding effects of an extended conformation. Sedimentation equilibrium (SE) analyses estimate mass independent of shape, and the concentration profile by this method was best fitted by a mass of ~114.7 kDa, consistent with pentameric assembly (Fig. 4c).

Electrostatic surfaces

The electrostatic properties of the N- and C-modules differ significantly. The N-module exhibits an uneven charge distribution with acidic (red) and basic (blue) patches (Fig. 1c and d). In contrast, acidic and basic residues in the C-module are secluded at the upper and lower portions, respectively. The most C-terminal acidic patches are within the β4–α6 turns (Glu165–Glu167) and β5–β6 loops (Glu196 and Asp197) at the top of the assembly. The β5–β6 loops crowning the C-terminal KCTD5 module are able to adopt well-defined conformations only when they interact with neighboring KCTD5 assemblies in the crystal lattice and refold in crystals formed in different ionic conditions (Fig. S1). In the absence of close packing contacts, electron density maps were poorly defined for two of the five β5–β6 loops in high salt (and four of the five in low salt), indicative of flexibility.

Electrostatic surfaces of residues that face the central cavity and at the interfaces between neighboring subunits are shown in Fig. 5a. Interface interactions in the N-module are mediated by polar residues, while those in the C-module are mostly hydrophobic. Similar to Kv channel T1 domains,[1,2] acidic and basic residues are isolated on opposite sides of the BTB domains in KCTD5, promoting circular side-to-side arrangement of subunits. In contrast, BTB folds in transcription factors lack polarized distribution of acidic and basic amino acids, and their dimeric assembly is performed via an additional N-terminal α-helix.[18] Pentamer assemblies of KCTD5 and the N-module alone are nearly equivalent, showing an average RMSD of ~0.8 Å. This suggests that the N-module has a lead role in homomeric assembly. Overexpression of the C-module (residues 154–234) led to accumulation of insoluble material in inclusion bodies consistent with an inability to coassemble, a finding noted by others.[19]

Intermolecular interfaces

Two neighboring subunits in the N-terminal module are shown from the center of the assembly in Fig. 5b. Adjacent subunits assemble via polar edges of all three layers of the BTB fold (L1, L2,

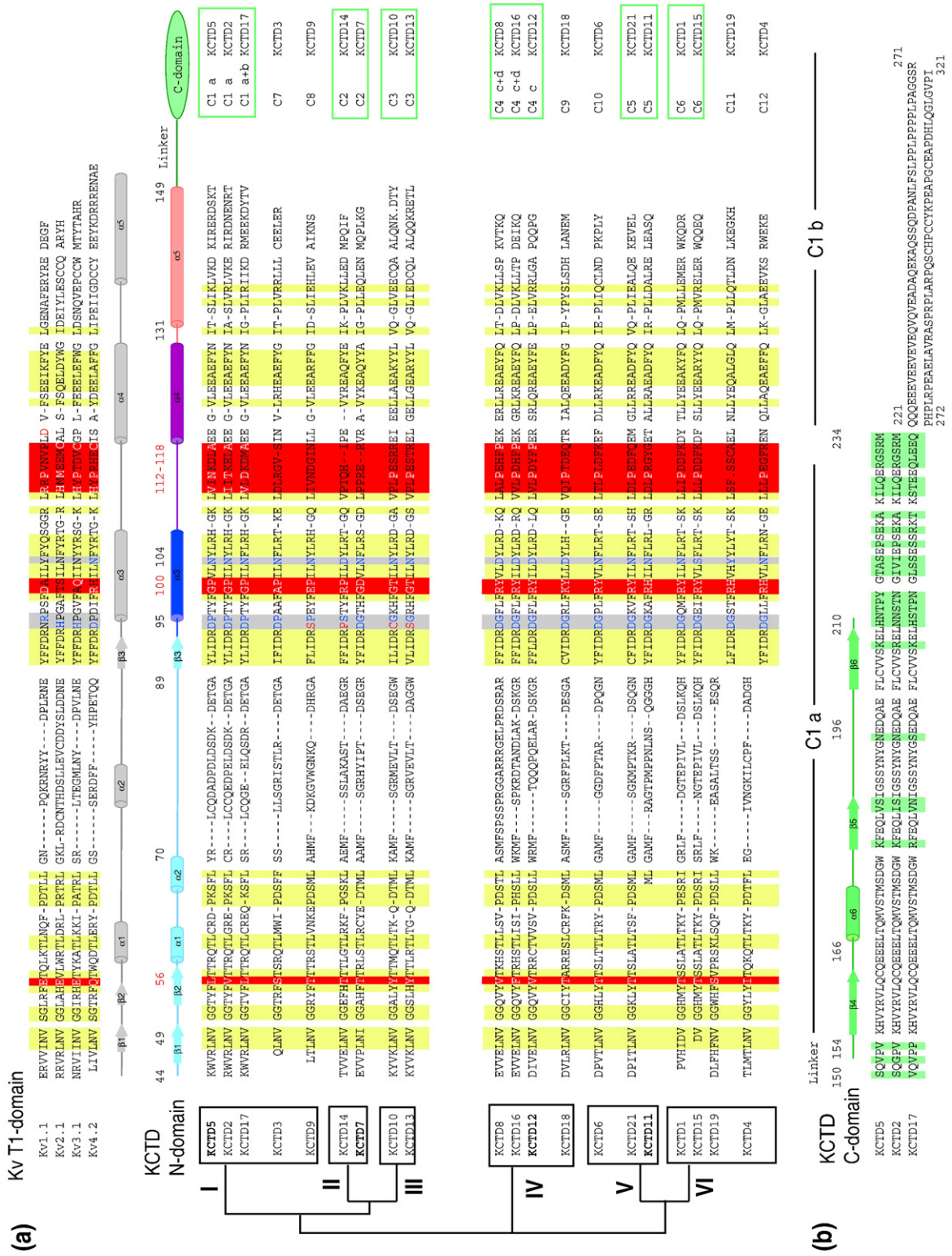

Fig. 3 (*legend on next page*)

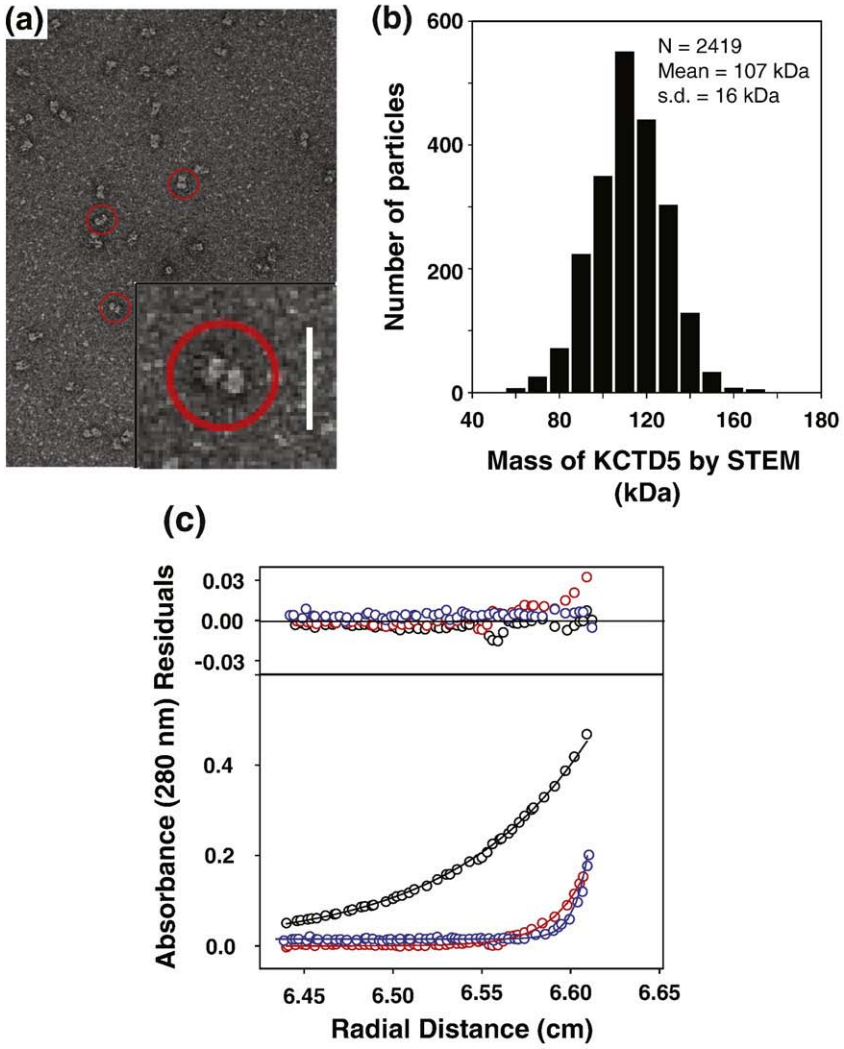

Fig. 4. Electron microscopic and analytical ultracentrifugation studies. (a) Electron micrograph of KCTD5 negatively stained with 2% (wt/vol) uranyl acetate shows particles with a two-domain architecture (circled) at a magnification of 72,000×. Inset: Scale bar represents 20 nm. (b) Histogram of the quantitative STEM mass analysis of KCTD5 (34–234) particles reveals mass distribution with a mean of 107 kDa. Scatter from individual particles ($N = 2419$) and conversion into absolute mass, as per Methods. s.d. = standard deviation. (c) SE data for KCTD5 (34–234) fitted using SEDPHAT. KCTD5 absorbance (280 nm) is shown at 12,000 rpm (black), 24,000 rpm (red), and 36,000 rpm (blue) for analyses with 0.35 mg ml^{-1}. The upper panel shows a residual difference between calculated fit and experimental data.

and L3), with β1–β2, β3–α3, and α4 residues of subunit 1 facing the β2, α3, and α3–α4 loop residues on subunit 2, respectively. Subunit 1 employs acidic Asp93 and Asp95 in the β3–α3 turn and Glu124 in α4 to interact via H-bonds with subunit 2 Arg107 in α3 and Lys110 in the α3–α4 loop. The interface surface is ~37 Å in length and ~22 Å in breadth, with a buried area for each subunit of ~710 $Å^2$. A

Fig. 3. Sequence and secondary structure alignments. KCTD BTB domains share a 33–43% sequence homology with T1 domains of Kv channels,[1,2] with most differences in the middle and C-terminus of the fold. Zinc-binding motifs in the T1 domains of Kv2, Kv3, and Kv4 channels are not found in KCTDs. (a) Alignment of the T1 domains of select Kv channels and KCTD N-terminal BTB domains based on X-ray structures: KCTD5 (this work), Kv1.1 (PDB ID 1T1D), Kv3.1 (PDB ID 3KVT), and Kv4.2 (PDB ID 1NN7). Secondary structure elements are those determined for Kv4.2 and KCTD5. Conserved patches are highlighted in yellow. Key differences are highlighted in red. The alignment of KCTD proteins was performed with ClustalW. KCTD20 is omitted. The schematic on the left is a KCTD group classification. Residues before the BTB domain are omitted. The KCTD5 N-terminal BTB fold is 106 residues long (residues 44–149). The consensus sequence (including insertions) is 110 amino acids long, with 26 residues in the diverse α2–β3 loop (corresponding to KCTD5 residues 70–89) and 14 residues in α5 (KCTD5 residues 132–149). Sequences of the α2–β3 loop and α5-helix display homology only between proteins of the same group. The C-termini of 14 KCTDs show significant identity with at least one other variant, while seven are distinct. The percent similarity of groups C1, C2, C3, C4, C5, and C6 are 88%, 50%, 93%, 69%, 48%, and 83%, respectively. (b) Alignment of KCTD5, KCTD2, and KCTD17 C-termini; differences are highlighted in green. Residues 212–234 are disordered in the KCTD5 crystal structure.

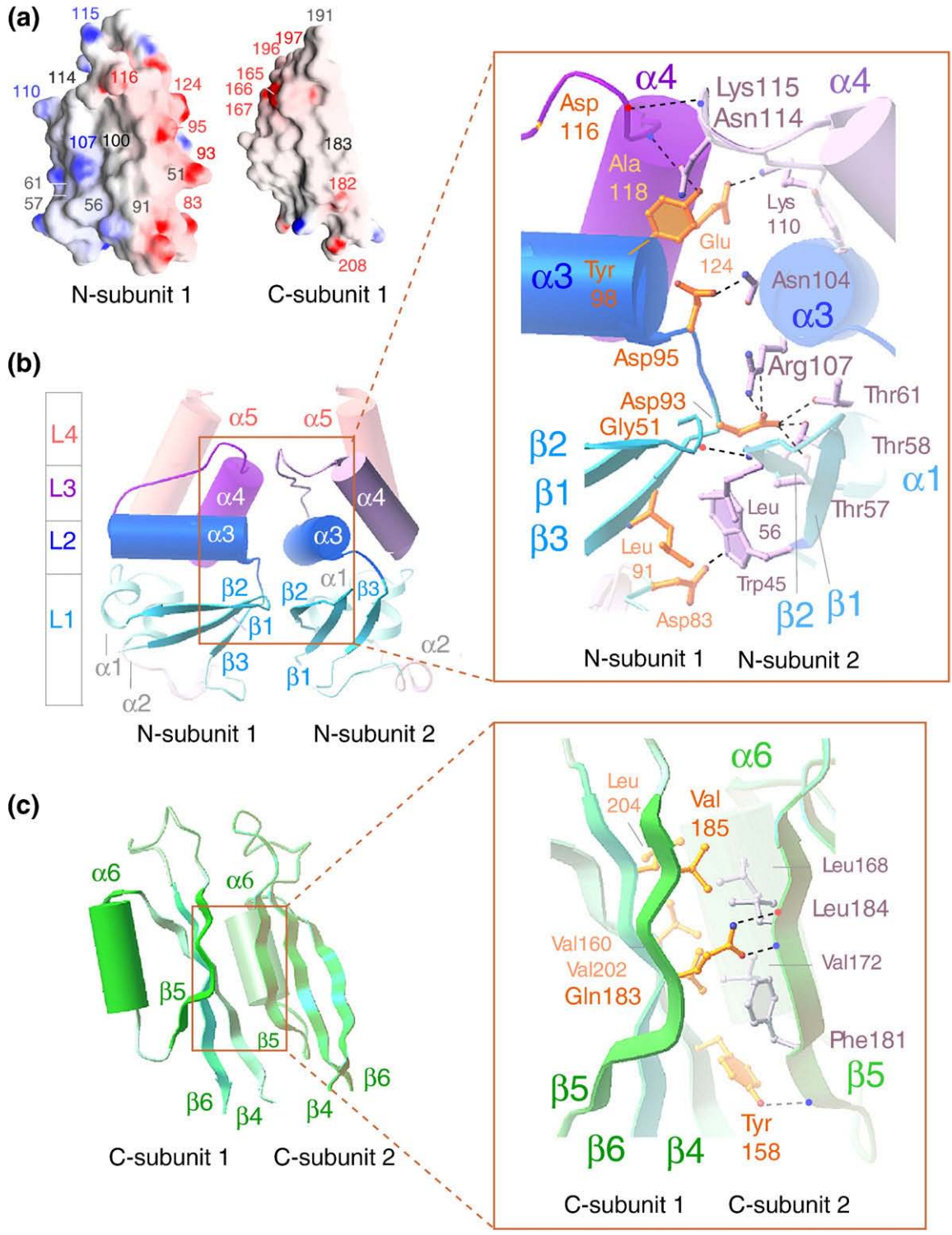

Fig. 5. Intermolecular interfaces in KCTD5 assemblies. (a) Potential surfaces of individual KCTD subunit N- and C-modules. Indicated in red are acidic Asp83, Asp93, Asp95, Asp116, Glu124, Glu165–Glu167, Glu196, Asp197, Glu182, and Glu208; basic residues Arg107, Lys110, and Lys115 are indicated in blue. Gly51, Leu56, Thr57, Thr61, Leu91, Gly100, Asn114, and Gln183 are noted in gray. (b) Secondary structural elements at the interface of adjacent subunits in the N-module viewed from the center of the assembly. α-Helices and β-strands are depicted as cylinders and arrows, respectively. The L1–L4 segments of the BTB fold are shown in colors as per Fig. 2. Inset presents an expanded view of the boxed area. Residues that form interfaces are shown in ball-and-stick in yellow (subunit 1) and gray (subunit 2). H-bonds (2.6–3.4 Å) are indicated with dotted lines. Asp116 (subunit 1) and Lys115 (subunit 2) interact via main-chain atoms, and their side chains are omitted for clarity. H-bond pairs and distances are noted in further detail in Fig. S2a. (c) Secondary structural elements at the interface of adjacent subunits in the C-module viewed from the center of the assembly as in (b). Inset presents an expanded view of the boxed area as in (b). H-bond pairs and distances are noted in further detail in Fig. S2b.

network of H-bonds between the subunits spans all three layers (Fig. 5b, inset; Fig. S2a).

The interface between neighboring subunits in the C-module is formed mainly by hydrophobic residues and shown from the center of the assembly in Fig. 5c. The interface surface is ~40 Å in length and ~16 Å in breadth, with a buried area of ~580 Å^2. The β-sheets 4–6 of one subunit lie against the α6–β5 junction of the adjacent subunit employing subunit 1 residues Tyr158, Val160, Val185, Val202, and Leu204, and subunit 2 residues Leu168, Val172, Phe181, and Ile184 (Fig. 5c, inset). The side chains of five Gln183 residues on β5 face the center of the assembly to shield hydrophobic residues and to shape the central cavity. This arrangement is stabilized by three H-bonds between the side chains of Tyr158 and Gln183 in subunit 1 and the main-chain atoms of Phe181 and Ile184 in subunit 2 (Fig. 5c, inset; Fig. S2b).

BTB folds of KCTD5 and Kv channel T1 domains

To assess how a fifth subunit is stably incorporated, KCTD5 was compared to the crystal structures

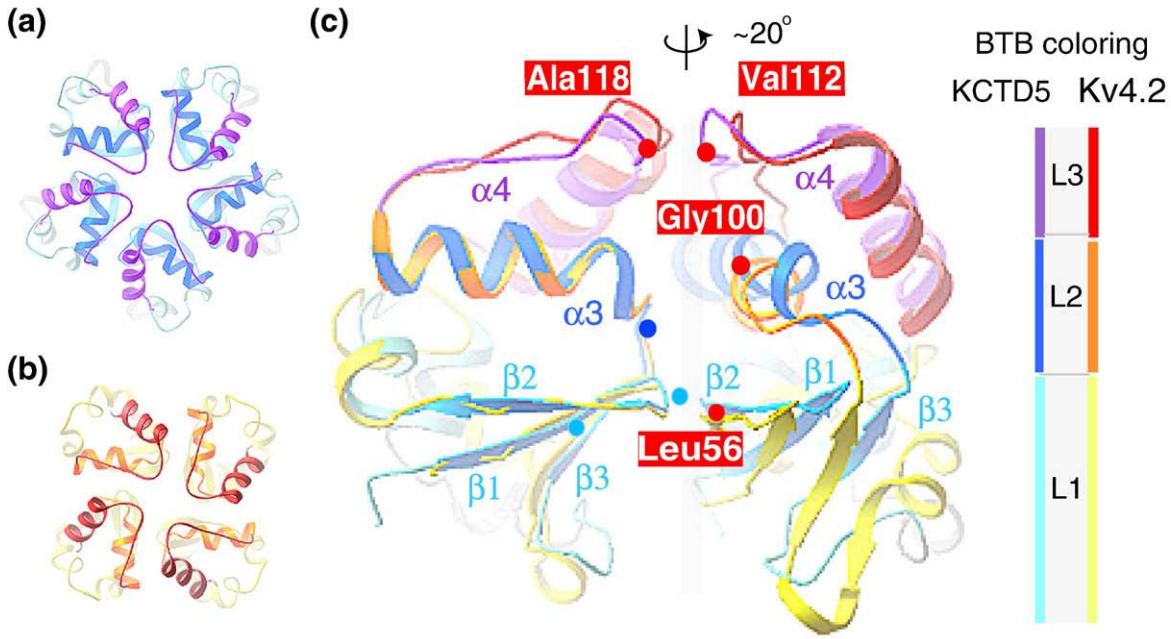

Kv1.1	Kv3.1	Kv4.2	KCTD5		KCTD5	Kv4.2	Kv3.1	Kv1.1
Asp^{140}	Cys^{81}	Cys^{111}	Ala^{118} α3-α4 loop	L3	α3-α4 loop Val^{112}	His^{105}	His^{75}	Arg^{132}
Arg^{115}	His^{58}	Asp^{88}	Asp^{95} β3-α3 loop	L2	α3-helix Gly^{100}	Arg^{93}	Gln^{64}	Asp^{119}
Ser^{73} Asn^{71}	Gly^{17} Asn^{15}	Ser^{48} Asn^{46}	Gly^{51} β1-β2 turn Asn^{49} β1-strand	L1	β2-strand Leu^{56}	Gln^{53}	Glu^{22}	Glu^{78}

Fig. 6. BTB protein–protein interfaces in KCTD5 and T1 domain assemblies. BTB layers are as follows: L1 in cyan (KCTD5) and yellow (Kv4.2); L2 in blue (KCTD5) and gold (Kv4.2); L3 in violet (KCTD5) and red (Kv4.2). L4 a5 helix is omitted for clarity. X-ray structures used: KCTD5 (high salt), Kv1.1 (PDB ID 1T1D), Kv3.1 (PDB ID 3KVT), and Kv4.2 (PDB ID 1NN7). (a) Top view of a pentameric assembly of KCTD5 N-modules. (b) Top view of a tetrameric assembly of Kv4.2 T1 domains. (c) Comparison of pairs of adjacent subunits for the KCTD5 N-module and the Kv4.2 T1 domain. To highlight the ~20° difference in orientation, subunit pairs were aligned on subunit 1 (left). C^{α} atoms of four key aliphatic residues in KCTD5 are noted (red spheres) and labeled; C^{α} atoms of their partners are in cyan (L1) or blue (L2). Inset: The correspondence of KCTD5 and T1 residues by layer with KCTD5 secondary structure elements is noted. Interface H-bond pairs and distances are presented in Fig. S2c.

of T1 tetramers in Kv1.1, Kv3.1,[15] and Kv4.2[20] (Figs. 6 and 7). While secondary structural elements are similar, KCTD5 and T1 differ in relative orientation by ~20° to accommodate five (Fig. 6a) or four (Fig. 6b) subunits. Superimposition of the interfacial regions of KCTD5 and the T1 in Kv4.2 revealed salient differences (Figs. 6c and 7; Fig. S2c). The BTB fold in KCTD5 has four aliphatic substitutions (Leu56 in β2, Gly100 in α3, and Val112 and Ala118 in the α3–α4 loop) at sites that are hydrophilic in T1 (Fig. 6c) and known to be important to formation of tetrameric assemblies.[15,20] KCTD5 employs other charge–charge interactions found in T1 domains, notably Asp93 (β3–α3 turn) and Glu124 (α4-helix) with Arg107 (α3-helix), and Lys110 (α3–α4 loop) at the interface between adjacent subunits (Fig. 5b).

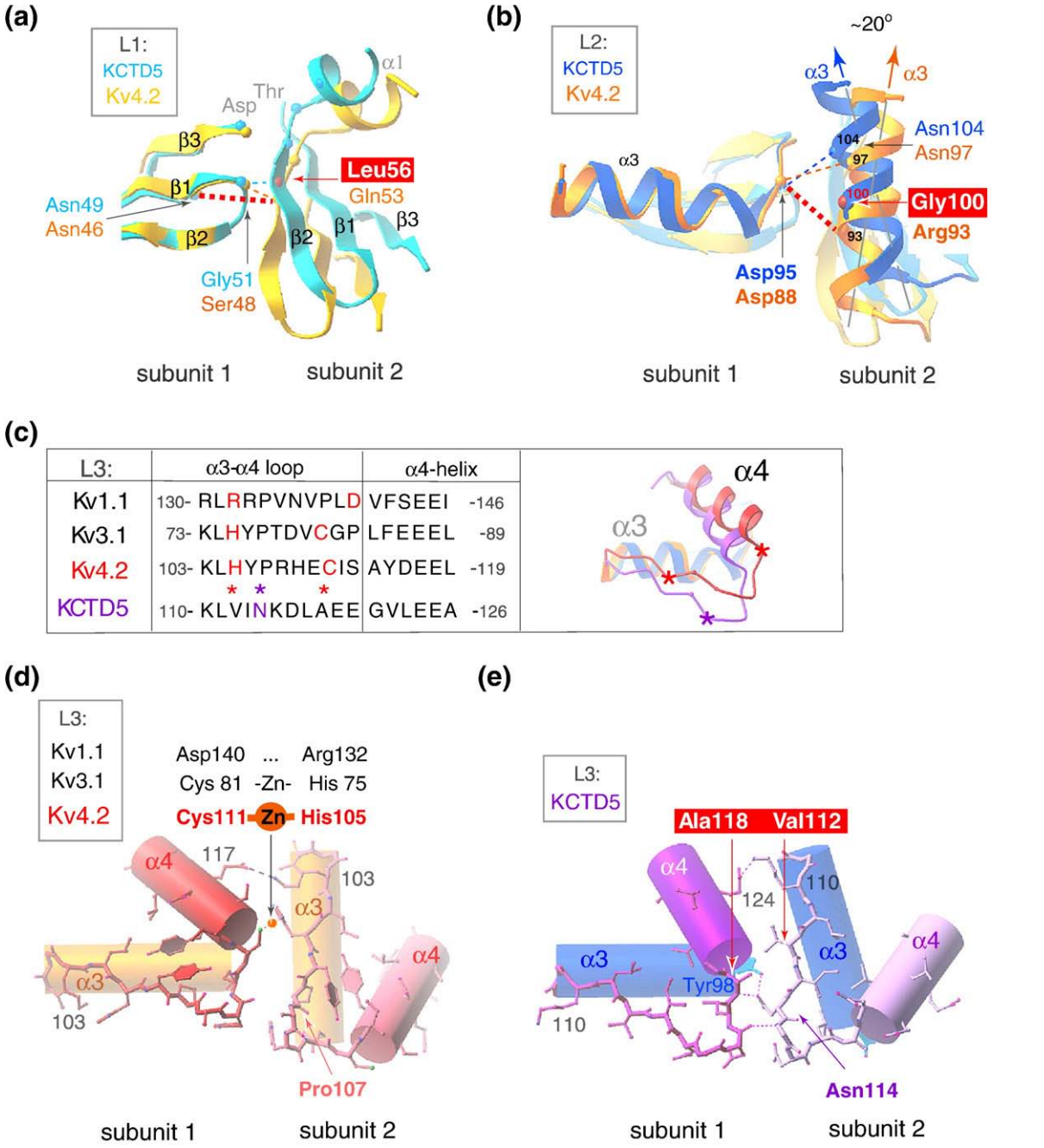

Fig. 7. BTB intramolecular interactions in KCTD5 and T1 domains. KCTD5 (high salt) and Kv4.2 (PDB ID 1NN7) structures are shown in the color scheme of Fig. 6. H-bonds are indicated as dashed lines. Four key residue differences between the KCTD5 and T1 interfaces are boxed. (a) BTB L1. Interacting residues shown as small spheres at the C^{α} atoms. The view is perpendicular to the image in Fig. 6c. (b) BTB L2. Presentation as in (a). The ~20° difference in orientation of the α3-helix axes of KCTD5 and Kv4.2 is indicated. (c). BTB L3 sequence alignment and ribbon presentation for KCTD5 and Kv4.2 viewed from the top. Val112, Ala118, and Asn114 in KCTD5 are marked with asterisks. (d) BTB L3 in Kv4.2 α3- and α4-helices is shown as cylinder, and the α3–α4 loop is shown in ball-and-stick mode. Arg108 side chain is omitted for clarity. (e) BTB L3 in KCTD5. Representation as in (d). Lys115 side chain is omitted for clarity.

At level L1 (Figs. 6c and 7a), KCTD5 Leu56 in the β2-strand (subunit 2) interacts with β1–β2 turn residue Gly51 (subunit 1) via the main-chain N-amino group, whereas in T1 domains, hydrophilic Gln or Glu in the β2-strand interacts via an H-bond network with a β1–β2 turn Ser or Gly and β1-strand Asn via main-chain and side-chain atoms, respectively. All KCTDs have the β1-strand Asn (Asn49 in KCTD5) found in T1 domains, but none has Gln (or Glu) in the β2-strand (Fig. 3).

At level L2 (Figs. 6c and 7b), KCTD5 bears Gly100 in the middle of α3 (subunit 2), whereas T1 domains have Arg, Gln, or Asp that forms an H-bond network with β3–α3 turn residues Asp, His, or Arg (subunit 1), respectively. KCTD5 does bear Asp95 at the end of the β3–α3 turn (analogous to Asp88 in

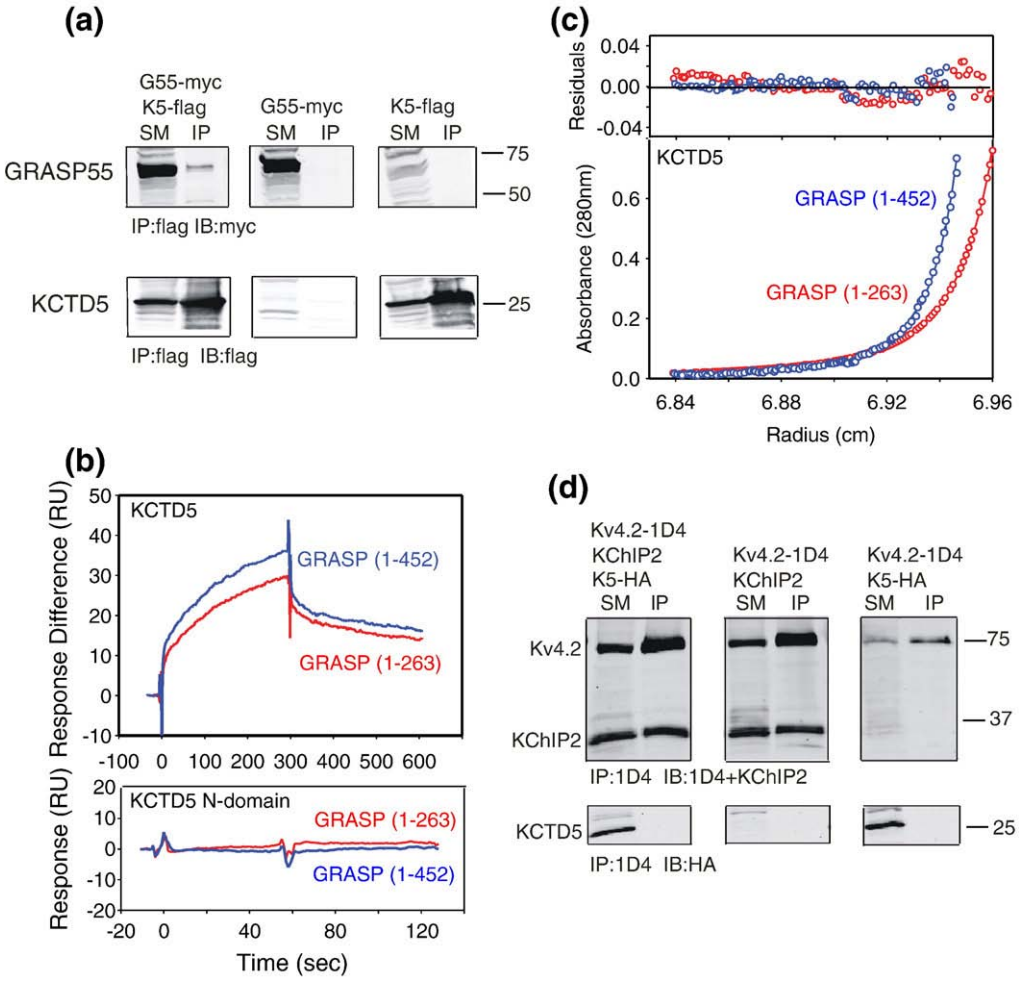

Fig. 8. Binding of KCTD5 and GRASP55 in solution. (a) KCTD5 (K5) copurifies with GRASP55 (G55) when coexpressed in HEK293 cells. Starting material (SM) was a detergent-soluble lysate that was incubated with antibody to FLAG to yield immunoprecipitate (IP); SM and IP were resolved by SDS-PAGE and visualized by Western blot analysis (IB) with antibody to myc or FLAG. Upper panels show that GRASP55 is isolated specifically with KCTD5 and is not seen either in the absence of KCTD5 or in the absence of GRASP55. Lower panels show that KCTD5 is isolated in complexes with GRASP55. Numbers indicate apparent mass (in kDa). (b) KCTD5 and GRASP55 studied by SPR. Upper panel depicts the binding of full-length GRASP55 (blue line) or truncated GRASP55 (residues 1–263; red line) to KCTD5 (residues 34–234) immobilized on the surface. GRASP proteins injected at 5 μM. Measured biophysical parameters are listed in Table 2. Lower panel shows that GRASP55 does not bind to the KCTD5 N-terminal domain. (c) Equilibrium sedimentation shows the association of KCTD5 and GRASP55. Here, KCTD5 residues 34–234 (9.2 μM) and full-length GRASP55 (blue line; 2.6 μM) or truncated GRASP55 (residues 1–263; red line; 2.5 μM) are shown at 24,000 rpm in the lower panel. The upper panel shows a residual difference between the calculated fit and experimental data. Nine data sets (three speeds and six concentrations) were analyzed globally using SEDPHAT 4.3 software (Methods), yielding equilibrium binding affinities of 1.41±0.26 and 8.26±1.6 μM for full-length and truncated GRASP55, respectively. The estimated partial specific volumes and solvent densities of KCTD5 with full-length and truncated GRASP55 were 0.733 $cm^3\ g^{-1}$ and 0.99823 g ml^{-1}, respectively. (d) Kv4.2 and KChIP2 form complexes, but not KCTD5 on coexpression in COS cells. Lysates were incubated with antibody to 1D4 and resolved by SDS-PAGE, and the interaction was visualized by Western blot analysis with antibodies to KChIP2 and HA. Upper panels show that KChIP2 is purified with Kv4.2. Lower panels show that KCTD5 does not coimmunoprecipitate with Kv4.2 in the presence or in the absence of KChIP2 despite synthesis of the protein. Numbers indicate apparent mass (in kDa).

Kv4.2), and this interacts with Asn104 (analogous to Asn97 in Kv4.2), but Gly100 in the next helical turn (rather than Arg93 in Kv4.2) lacks the capacity to contribute to the network (Fig. 7b). As a result, the KCTD5 α3 helix tilts by ~20° compared to T1.

At level L3 (Figs. 6c and 7c–e), the V-shaped α3–α4 loop in KCTD5 differs significantly from T1 domains. Here, Kv4.2 and Kv3.1 deploy Cys and His, respectively, to bind zinc, and Kv1.1 bears Asp and Arg to form a salt bridge (Fig. 7c and d). In contrast, KCTD5 bears the small aliphatic residues Ala118 and Val112 at these sites (Fig. 7e). In KCTD5, the main-chain amino group in Ala118 (subunit 1) forms an H-bond with the carbonyl group of Asn114 (subunit 2). In addition, the Asn114 amide interacts with the hydroxyl of α3 residue Tyr98 (subunit 1). The H-bond network propagates to the tip of the α3–α4 loop via the main-chain carboxyl and N-amino groups of Asp116 (subunit 1) and Lys115 (subunit 2), respectively. As a result, the L3 segment rotates in KCTD5 relative to T1 (Fig. 7c)—a difference that appears to be favorable due to the absence of bulky aliphatic side chains present in T1 (Tyr *versus* Ile113, and Phe *versus* Val122) and the presence of Gly121 in α4 that stacks on top of the side chain of Tyr98 and interacts with Asn114. The KCTD5 α3–α4 loop sequence is homologous only to KCTD2 and KCTD17 (Fig. 3).

Thus, incorporation of a fifth subunit in the KCTD5 assembly is facilitated by four aliphatic substitutions compared to T1 domains: Leu56 and Gly100, which lead to loss of two H-bonds and relaxation of the interface at L1 and L2 (Fig. 7a and b), and Val112 and Ala118 (Fig. 7c–e), which allow adjacent L3 segments to come closer (~1 Å) in KCTD5 (Fig. 6c) and eliminate zinc-binding or salt-bridging T1 residues. It is interesting to note how KCTD maintains stability despite losing these interactions. KCTD5 employs Asn114 to bridge L3 to L2 on adjacent subunits via Ala118 and Tyr98 (Figs. 5b and 7e); Asp93 is held within a pocket formed by Thr57, Thr58, Thr61, and Arg107 in L1 of the neighboring subunit (Figs. 5b and 7b; Fig. S2a); the L1–L2 interface is stabilized by the interaction of Trp45 with Asp83 and Leu91 on the next subunit (Fig. 5b); and, as in T1, Glu124 and Lys110 at the periphery of L3 interact on flanking subunits (Fig. 7e).

The KCTD5 C-terminus is important for interaction with GRASP55

GRASP proteins contribute to the stacked organization of Golgi cisternae and are thought to participate in protein trafficking.[21,22] As reported by others,[13] we found that GRASP55 and KCTD5 expressed in the human embryonic kidney cell line 293T (HEK293) coimmunoprecipitate (Fig. 8a). Surface plasmon resonance (SPR) and SE analyses were therefore used to study the interaction of the purified proteins.

KCTD5 was observed by SPR to bind with micromolar affinity to both full-length GRASP55 and the GRASP55 N-terminal domain (residues 1–263), in accord with a simple 1:1 binding model (Fig. 8b, upper panel; Table 2). This argued for the assembly of one KCTD5 pentamer and one GRASP55 monomer, with an apparent equilibrium affinity of ~1 μM. Indicating that binding requires an intact KCTD5 C-module, the pentameric KCTD5 N-module (residues 40–145) bound neither full-length nor truncated GRASP55 (Fig. 8b, lower panel; Table 2).

Analytical ultracentrifugation at three speeds and nine protein concentrations, analyzed using SEDPHAT 4.3, indicated masses of ~172 and ~147 kDa for complexes of KCTD5 with full-length and truncated GRASP55 protein, respectively (Fig. 8c). These are the expected values for KCTD pentamers and a GRASP55 monomer, respectively, based on masses of ~115, 48, and 28 kDa for KCTD5, full-length GRASP55, and truncated GRASP55. The concentration profile gave a good fit with a single site model to yield an equilibrium binding affinity of 1.41±0.26 and 8.26±1.6 μM for full-length and truncated GRASP55, respectively, in keeping with the affinity estimation by SPR.

KCTD5 does not alter the function of four Kv channel subtypes

Kv channels require a multitude of regulatory accessory subunits to operate *in vivo*,[6] and KCTD proteins were expected to serve this purpose. To our surprise, electrophysiological and biochemical methods failed to support expectations. KCTD5 shares sequence homology with the BTB-bearing T1 domains of Kv channels, most significantly those in the Kv4 subfamily (Fig. 3). Whereas KCTD5 was without effect on Kv4.2, the known regulator Kv channel interacting protein 2 (KChIP2) that interacts via the channel N-terminus[23] in *Xenopus laevis* oocytes increased current density, slowed inactivation, and speeded recovery from inactivation (Table 3). Furthermore, the effects of KChIP2 were unaltered by coexpression with KCTD5. Similarly, KCTD5 neither impacted directly nor interfered with KChIP2

Table 2. SPR (Biacore) kinetic data for KCTD5 and GRASP55 binding

Immobilized protein	Injected protein	k_a (M^{-1} s^{-1})	k_d (s^{-1})	K_D (M^{-1})
$KCTD_{34–234}$	$GRASP55_{1–452}$	$0.87\pm0.1\times10^{3}$	$1.03\pm0.2\times10^{-3}$	$1.18\pm0.2\times10^{-6}$
$KCTD_{34–234}$	$GRASP55_{1–263}$	$2.59\pm0.4\times10^{3}$	$2.23\pm0.4\times10^{-3}$	$8.6\pm1.2\times10^{-7}$

$KCTD_{40–145}$ (the N-module assembly) bound neither $GRASP_{1–452}$ nor $GRASP55_{1–263}$.
k_a: Association rate constant; k_d: dissociation rate constant; K_D: equilibrium binding constant.

Table 3. Biophysical properties of Kv channels expressed with KCTD5

	Kv4.2	Kv4.2+KCTD5	Kv4.2+KChIP	Kv4.2+KCTD5+KChIP	Kv3.4	Kv3.4+KCTD5
Peak current (μA at 40 mV)	4.7±1.0	3.9±1.0	5.2±1.2	4.8±0.9	1.9±0.8	2.3±0.6
Time to peak (ms at 40 mV)	8.2±1.1	7.9±0.8	9.2±1.1	9.4±1.0	9.3±0.3	9.7±0.6
Activation $V_{0.5}$ (mV)	−28±2	−25±2	−29±5	−28±3	7.8±2.3	8.2±1.1
Inactivation ($t_{0.5\ decay}$; ms at 40 mV)	25±4	24±5	48±6*	49±2*	8±1	8±1
Inactivation $V_{0.5}$ (mV)	−64±1	−62±3	−56±2*	−56±1*	−51±4	−50±4
Recover inactivation (τ; ms at 40 mV)	109±6	111±9	22±3*	23±2*	—	—

	Kv2.1	Kv2.1+KCTD5	Kv1.2	Kv1.2+KCTD5
Peak current (μA at 40 mV)	7.9±1.0	7.1±0.7	2.3±0.9	1.8±0.6
Activation (τ; ms at 40 mV)	2.7±0.3	2.4±0.1	4.3±0.6	4.0±0.5
Activation $V_{0.5}$ (mV)	2±3	2±2	−20±3	−20±4
Deactivation (τ_{fast}; ms at 40 mV)	3.1±0.3	3.6±0.3	4.5±0.8	4.9±0.5
Deactivation (τ_{slow}; ms at 40 mV)	63±7	63±5	49±9	50±7
Deactivation $a_f/(a_f+a_s)$	0.046±0.003	0.055±0.007	0.087±0.014	0.091±0.005

Data are presented as mean±SD for six to nine *Xenopus* oocytes injected with cRNA for the indicated proteins and using a two-electrode voltage clamp after 24 h of expression at room temperature. A 1:5 ratio for channel/KCTD cRNA was used, except for Kv3.4 (where a ratio of 1:1 was used) or in cells withKChIP2 (where the channel cRNA wasdecreased by 20-fold to compensate for KChIP2-induced increase in surface expression). KChIP2 slows inactivation and speeds recovery from inactivation of Kv4.2 channels in the presence or in the absence of KCTD5.

Voltage protocols and curve fits are as described in Methods.

* $P<0.001$ (by t test).

regulation of Kv4.2 channels studied in Chinese hamster ovary (CHO) cells using whole-cell patch clamp (not shown). Moreover, KCTD5 had no effect on the biophysical operation of three other Kv channels from additional subfamilies with BTB motifs: Kv1.2, Kv2.1, and Kv3.4.

When KCTD5, KChIP2, and Kv4.2 were expressed in African green monkey COS-7 cells using methods we have previously employed,[24] KChIP2 was copurified with Kv4.2, while KCTD5 was not isolated with Kv4.2 whether or not KChIP2 was present in the cells (Fig. 8d). The same observations were made with CHO cells and for studies with Kv4.3 channels (not shown).

Discussion

We report the X-ray crystal structure of human KCTD5, the first member of the family to be so characterized. The structure reveals a gown-shaped pentameric assembly with N- and C-modules and a central complex-spanning cavity (Figs. 1 and 2). Comparing two crystal forms revealed that the modules can swivel by ~30° around the intermodule linker (Fig. 1b and d). Coiled coils show unusual versatility allowing the assembly of subunits with more than one stoichiometry using the same portion of the fold.[14] While BTB motifs had previously been demonstrated to mediate aggregation of two and four subunits via separate portions of the domain,[7] we demonstrate here that the same BTB surfaces mediate pentamer and tetramer formation in KCTD5 and Kv channels, respectively (Figs. 6 and 7).

While the BTB in KCTD5 preserves many interactions found in T1 domains to array polar edges at subunit interfaces (Fig. 5b), it has four aliphatic substitutions that allow incorporation of a fifth subunit (Figs. 6 and 7): Leu56 in L1, Gly100 in L2, and Val112 and Ala118 in L3; these sites in T1 domains are hydrophilic and important for tetrameric assembly.[15,20] As a result, KCTD5 lacks two H-bonds and one ionic interaction, relaxing the intersubunit interface. Moreover, Val112 and Ala118 permit adjacent subunits to come closer than in T1 domains and eliminate zinc-binding or salt-bridging residues at the corresponding positions.

The high sequence identity (>70%) of KCTD5 with the N-termini of KCTD2 and KCTD17 suggests that the latter will also form pentameric assemblies. Although KCTD3 and KCTD9 bear only ~60% homology in the BTB domain with KCTD5 and have unique C-termini, we suspect that they also will form pentamers because they are more similar to KCTD5 than T1 domains (Fig. 3). The number of subunits in other KCTD complexes is less apparent because, for example, groups IV–VI have Arg where KCTD5 has Gly100 in α3 (Fig. 3).

Testing was far from exhaustive; however, we gathered no evidence that KCTD5 assembles with or influences the function of Kv channels. Sequence similarities suggest that like KCTD5, KCTD2, KCTD3, and KCTD17 will be without effect on Kv4.2, Kv3.4, Kv2.1, and Kv1.2. The 21 *KCTD* genes predict proteins that can be sorted into seven groups based on the alignment of their N-terminal sequences (Fig. 3). Some *KCTD* genes are single-exon loci (4, 11, 12, and 14), while others appear to be subject to splice variation that would increase diversity. Group I contains KCTD 2, 3, 5, 9, and 17. KCTD5 is most closely related to KCTD2 and KCTD17, with ~70% and ~80% identity to their N- and C-modules, respectively, while KCTD3 and KCTD9 display ~60% similarity to the KCTD5 N-module and have dissimilar C-termini. The KCTD5 N-module displays ~20% identity (~40% similarity) to the T1 domains of Kv1, Kv2, Kv3, and Kv4 channels.

KCTD5 does assemble with GRASP55.[13] Purified human KCTD5 and GRASP55 showed an affinity of ~1 μM by SPR and SE (Fig. 8b and c). The KCTD5 N-module forms pentameric complexes on its own, but does not bind GRASP55, supporting a role for the C-terminus.

KCTD5 reveals a novel fold in the C-module composed of aligned β4/α6 and β5/β6 hairpins that expose loop residues to solvent (Fig. 1; Fig. S1). This domain may be involved in assembly with GRASP55 via an electronegative patch atop the module (Glu196 and Asp197 in the β5–β6 loop and Glu165–Glu167 in the β4–α6 turns; Fig. 1c and d; Fig. S1), and Tyr and Ser in the β5 and β6 loops (residues that are important in other flexible loops for protein–protein recognition).[25,26] KCTD5 crystal structures in high salt and low salt demonstrate flexibility of the β5 and β6 loops (Fig. S1). The KCTD5 C-module also appears to have a role in binding the adenoassociated virus type 2 proteins Rep78 and Rep68 because removing the last 31 residues of KCTD5 blocks Rep protein binding and nuclear accumulation.[27] The rotational flexibility of KCTD5 intermodule linker and refolding of the loops crowning the C-module suggest that these changes may be required to bind and respond to ligands.

Methods

Cloning, expression, and purification

DNA for human KCTD5 (NP_061865) was amplified by PCR from adult brain cDNA (Clontech, Palo Alto, CA), inserted into TOPO 2.1 (Invitrogen, Inc., Carsbad, CA), and subcloned into pMax, an in-house dual-purpose expression vector containing a Cytomegalovirus promoter for mammalian expression and a T7 promoter for cRNA synthesis. For biochemistry and electrophysiology studies, KCTD5 (residues 1–234) constructs with and without an N-terminal epitope tag for hemagglutinin A (HA) were used, respectively. For structural and binding analyses, truncated versions of KCTD5 carrying residues 34–234 ("full length") or 40–145 ("N-module") were produced; these were subcloned into a modified pET28a vector (Invitrogen, Inc.) with six His residues and a TEV protease cleavage site replacing the thrombin site and then expressed in *Escherichia coli* BL21(DE3) (Novagen, Madison, WI). Selenomethionine-labeled proteins were produced as described.[28] Native and selenomethionine-labeled proteins were purified on Ni^{2+}-NTA affinity columns (Qiagen, Valencia, CA), subjected to TEV protease cleavage, further purified through a second Ni^{2+}-NTA column and gel filtration on a Superdex-200 column (GE Healthcare, Piscataway, NJ), and equilibrated with 50 mM Tris–HCl (pH 7.5), 150 mM NaCl, and 2 mM DTT. The KCTD5 C-terminal residues 154–234 were expressed in the same *E. coli* strain and found exclusively in inclusion bodies. Human GRASP55 (NP_056345) was produced with residues 1–452 and 1–263 in the same manner.

Crystallization and data collection

Crystals were produced by the hanging-drop diffusion technique at 19 °C using 20 mg ml^{-1} protein. Preliminary crystallization screening was performed with the INDEX screen (Hampton Research, Aliso Viejo, CA). After several rounds of optimization, two crystal forms of KCTD5 were obtained: high salt [3.2 M NaCl and 100 mM Tris–HCl (pH 8.5)] and low salt [0.2 M proline, 100 mM Hepes (pH 7.5), and 7% (wt/vol) polyethylene glycol 3350]. The N-terminal KCTD5 domain was crystallized in 24% (wt/vol) polyethylene glycol 3350, 100 mM $MgCl_2$, and 100 M Hepes (pH 7.5). Crystals were cryoprotected in the presence of glycerol (22–25%, vol/vol) or mineral oil and flash-frozen in liquid nitrogen. X-ray diffraction experiments were performed at 100 K using the GM/CA CAT 23IDD beamline of the Advanced Photon Source (Argonne National Laboratory, Argonne, IL). X-ray data sets were processed and scaled with HKL2000.[29]

Structure determination and validation

The structure was solved by SAD on the high-salt crystal form of the selenomethionine-labeled full-length KCTD5. A heavy-atom search was performed in SHELXD[30] using a 3.5 Å X-ray resolution cutoff. SAD phasing, electron density modification, and noncrystallographic (fivefold) averaging were performed in the SOLVE/RESOLVE suite.[31,32] The initial model building allowed ~25% of the main-chain atoms with the RESOLVE basic script. The electron density map and autobuilt model were examined in TURBO-FRODO.[33] Model building of the C-terminal domain that bears two selenomethionine residues (M171 and M175) was completed first. SAD and calculated phases from the C-terminal domain allowed improvement of the electron density and completion of the model for the N-terminal region that has no Met residues. Simulated annealing and preliminary positional refinement were performed in CNS1.1.[34] The N-module was used to solve the crystal structure of the truncated N-terminal domain by molecular replacement using MOLREP.[35] The structure of the N-terminal domain was then refined at 1.9 Å X-ray resolution in REFMAC5[36] using the protocol implemented in CCP4[37] that included the search for water molecules, restrained positional and individual *B*-factor refinement, and TLS (*t*ranslation, *l*ibrations, and *s*crew axis rotation) and bulk solvent parameter refinement and electron density map calculations. After refinement, the structure of the N-terminal domain was used to verify the model of the N-terminal domain in the high-salt crystal form of the selenomethionine-labeled full-length KCTD5. The corrected model of the full-length KCTD5 was then refined in REFMAC5 using noncrystallographic symmetry and a protocol that included the restrained positional and *B*-factor refinement, followed by the TLS and bulk solvent parameter refinement. The low-salt crystal structure of the native full-length KCTD5 was solved by molecular replacement using the refined N- and C-terminal pentameric modules from the high-salt crystals as trial models in the dyad search implemented in MOLREP. The refinement was carried out in REFMAC5 using a protocol similar to that used to refine the high-salt crystal form. Crystal data, X-ray data collection, and refinement statistics are listed in Table 1. During refinement, R_{free} was monitored by setting aside 5% of the reflection as test set. A Ramachandran plot calculated in CCP4 indicated that 100% of non-Gly and non-Pro residues in the N-terminal KCTD5 structure lie in the most favored or additionally allowed regions. The full-length KCTD5 structures have 99.1% (high-salt KCTD5) and 97.7% (low-salt KCTD5) of non-Gly and non-Pro residues in the most favored or additionally allowed regions, with others in the generously allowed regions of the Ramachandran plot and

only partially ordered in the crystal structures. These residues belong to the loop adjoining the α2-helix and β5 and β6 loops. Residues 188–199 constituting β5 and β6 loops adopt well-defined conformations only when they interact with the neighboring protein molecules in the crystal lattice. The packing arrangements are different in the two crystal forms for KCTD5. A more pronounced involvement of the β5 and β6 loops in the crystal packing was found in the high-salt form, where three loops were defined in the electron density maps and modeled. The sigmaA-weighted $2F_{obs}-F_{calc}$ electron density map is shown in Fig. S1e. In contrast, only one subunit exhibits partially ordered β5–β6 conformation in low-salt crystals and is unlike the high-salt structure.

Surface area calculations were performed using the Protein–Protein Interaction Server‡. The central cavity was calculated using the HOLE program.[38] The three-dimensional figures were calculated using RIBBONS.[39] The potential surface was prepared using the program GRASP.[40]

Sequence analysis

Classification of KCTD proteins into groups I–VI was performed by multiple sequence alignment in ClustalW2§ and then confirmed by sequence identity/similarity calculations in pairwise alignment with EMBOSS.[41] Sequence alignment between human KCTD proteins and Kv T1 domains was performed with ClustalW2 and confirmed based on X-ray crystal structures (Fig. 3): KCTD5 (this work), Kv1.1 (PDB ID 1T1D), Kv3.1 (PDB ID 3KVT), and Kv4.2 (PDB ID 1NN7).

Electron microscopy

For negatively stained imaging, purified KCTD5 was diluted to a concentration of 0.17 mg ml^{-1} in 200 mM NaCl and 20 mM Tris–HCl (pH 7.5) with 2 mM DTT and stained with 2% (wt/vol) uranyl acetate over a glow discharge thin carbon film. Images were recorded on a charge-coupled device with a FEI Morgagni microscope at an acceleration voltage of 80 keV, a magnification of 72,000×, and a defocus of 1 μm, giving a pixel size at the specimen level of 3.33 Å.

Quantitative mass analysis by STEM was performed at the Brookhaven National Laboratory (Upton, NY) with a custom-built electron microscope. Purified KCTD5 was diluted to 0.05 mg ml^{-1} in 150 mM NaCl and 10 mM Hepes (pH 7.4) with 1 mM DTT. Grid preparation and image acquisition were also performed‖. Data were analyzed using PCMass29 with a customized model for KCTD5. A total of 2149 particles were automatically selected from 50 images and processed. The KCTD5 measurements were calculated using Tobacco mosaic virus calibration for each image. Histogram generation and statistics were performed by SigmaPlot9.0.

Analytical ultracentrifugation

SV and SE experiments were carried out using an Optima XL-A analytical ultracentrifuge (Beckman Coulter, Fullerton, CA) equipped with a Ti60 rotor. SV data for KCTD5 (residues 34–234 or 40–145) and GRASP55 (full length or residues 1–263) were obtained at 40,000 rpm using an Epon two-channel centerpiece. Absorbance of the samples at 280 nm was monitored in a continuous-mode time interval of 360–480 s and a step size of 0.003 cm. Multiple scans at different time points were fitted to the continuous size distribution [$c(s)$] model using SEDFIT 11.3. The partial specific volume of the proteins and buffer density were calculated using SEDNTERP.

SE experiments were conducted at rotor speeds of 12,000, 24,000, and 36,000 rpm at 25 °C. Data were acquired as an average of 10 absorbance measurements at wavelengths of 230 and 280 nm, depending on the concentration of the proteins, and at a radial spacing of 0.001 cm. Molecular mass determination of KCTD5 (34–234) was performed at 0.1, 0.35, and 0.5 mg ml^{-1} in 150 mM NaCl and 10 mM Hepes (pH 7.4). For binding experiments, KCTD5 and GRASP55 were determined in 150 mM NaCl and 10 mM Hepes (pH 7.4). Ultrascan9.1 software was used to determine the time necessary to reach equilibrium at all three speeds: 38, 12, and 6 h, respectively. Nine data sets (three speeds and six concentrations) were analyzed globally using SEDPHAT 4.3 software. Protein concentrations were determined by absorbance at 280 nm using extinction coefficients of 2.62×10^4 M^{-1} cm^{-1} for KCTD5 and 2.71×10^4 M^{-1} cm^{-1} for both full-length and truncated GRASP55.

Coimmunoprecipitation

Mammalian expression constructs for GRASP55 and KCTD5 expressing epitope tags for myc and flag, respectively, were generously shared by A. Pandey, and coimmunoprecipitations were performed in accordance with Gandhi *et al.*[13] Briefly, cDNAs were cotransfected into HEK293 cells at a ratio of 1:1 μg using Lipofectamine 2000 (Invitrogen, Inc.) and lysed after 48 h. Proteins were solubilized in 1% NP-40 and clarified by centrifugation at 16,000*g* for 10 min. The supernatant was subjected to immunoprecipitation overnight with mouse anti-flag M2 affinity gel (Sigma) and SDS-PAGE electrophoresis. Western blot analyses with rabbit anti-c-*myc* antibody (1:200 dilution; Sigma) and goat anti-rabbit Alexa Fluor 680-nm fluorescent secondary antibody (1:5000 dilution; Invitrogen, Inc.) were imaged using LI-COR Odyssey (LI-COR Biosciences, Lincoln, NE). As described previously,[23,42] hKv4.2 (AH009258) expressing an epitope tag for 1D4 and untagged hKChIP2 (AAF33683) were transfected with HA-tagged hKCTD5 into CHO or COS-7 cells at a ratio of 1:2:2 Kv4.2/KChIP/KCTD5 and lysed after 48 h. Protein was solubilized in 1% Triton for 1 h and clarified by centrifugation at 50,000*g* for 30 min. The supernatant was subjected to immunoprecipitation overnight with anti-mouse monoclonal 1D4 and SDS-PAGE. Western blot analyses with rat anti-HA (1:1000 dilution; Roche) and mouse-anti KChIP2 (J. Trimmer, University of California, Davis, CA), Alexa Fluor 680-nm and 800-nm fluorescent secondary antibodies (Invitrogen, Inc.), and LI-COR Odyssey were used.

SPR binding

The interaction of KCTD5 and GRASP55 was analyzed by SPR using optical biosensor Biacore 3000 (GE Healthcare) at 25 °C. KCTD5 (34–234 or 40–145) was covalently coupled to the dextran surface of CM5 biosensor chips to a density of 4000–5000 response units using amine chemistry (per protocol). Purified full-length GRASP55 or residues 1–263 in running buffer [150 mM NaCl, 20 mM Hepes

‡ http://www.biochem.ucl.ac.uk/bsm/PP/server
§ www.clustal.org
‖ http://www.biology.bnl.gov/stem/stem.html

(pH 7.4), and 0.005% (vol/vol) surfactant P20] were applied over immobilized KCTD5 by injection (in triplicate) of various concentrations (0.1–5 μM) using a flow rate of 20 μl min^{-1}. Data were prepared by "double referencing," where parallel injections of analyte over a control dextran surface were performed, as well as by running buffer injections over both the immobilized KCTD and control dextran surfaces. In the derived sensogram, association and dissociation were fitted locally and globally using BIAevaluation 4.1 software (GE Healthcare). Affinity constants were estimated by fitting the data to a simple 1:1 binding model[43] and analyzed using $dR/dt = k_a C(R_{max} - R) - k_d R$, where R is the SPR signal (in response units); k_a is the association rate constant (in M^{-1} s^{-1}); k_d is the dissociation rate constant (in s^{-1}); C is the concentration of GRASP55 (in M); R_{max} is the maximum GRASP55 binding capacity (in response units); and dR/dt is the rate of change of the SPR signal. The equilibrium binding constants (K_D) of the complexes were determined as the ratio of k_a/k_d. The concentrations of purified proteins were determined by absorbance at 280 nm using the calculated extinction coefficients noted above. To confirm the specificity of KCTD5/GRASP55 binding, the following purified proteins were used: KChIP2 (residues 73–252), rat MiRP2 (NP_071571; residues 1–61), human SUMO1 (NP_001005781; residues 1–97), and bovine serum albumin (Pierce, Rockford, IL). There was no binding observed between these proteins and immobilized full-length KCTD5.

Electrophysiology

As described previously,[42] cRNA for Kv channels and KCTD5 were made using the T7 cDNA synthesis kit (Ambion) and injected into *X. laevis* oocytes. When hKChIP2 was included, channel cRNA was diluted 20-fold. The recording solution comprised 96 mM NaCl, 2 mM KCl, 1 mM $MgCl_2$, 1.8 mM $CaCl_2$, and 5 mM Hepes–NaOH (pH 7.5) for Kv4.2 recordings, and 96 mM NaCl, 4 mM KCl, 1 mM $MgCl_2$, 0.3 mM $CaCl_2$, and 10 mM Hepes–NaOH (pH 7.5) for all other channels. Electrodes were filled with 3 M KCl and had resistances of 0.2–0.5 MΩ. All experiments were performed at room temperature at 20–38 h postinjection. Voltage families were obtained with test pulses of −100 to 60 mV for 0.5 or 1 s with 10-mV increments every 10 s, using p/4 protocols. Time to peak current was used as a measure of activation, and time to half-maximal decay was used as a measure of inactivation for Kv3.4 and Kv4.2 channels. For Kv1.2 and Kv2.1 channels, activation was fitted with a single exponential equation, and deactivation was fitted with a double exponential equation. Steady-state inactivation was examined from a holding potential of −100 mV with test pulses from −120 to 10 mV held for 2.5 s, with a second pulse to −40 mV to measure currents that were not inactivated. $V_{0.5}$ activation and $V_{0.5}$ inactivation were calculated by fitting normalized conductance–voltage relationships with a Boltzmann function.[44] Recovery from inactivation was measured by driving channels to an inactivated state at 40 mV, hyperpolarizing to −110 mV, and then applying a second pulse to 40 mV for 10-ms incremental intervals. Recovery from inactivation was fitted with a single exponential equation. All parameters were analyzed and averaged with six to nine cells per group.

Accession codes

Coordinates and structure factors have been deposited in the PDB with PDB codes 3DRX, 3DRY, and 3DRZ. The following accession numbers were also used: human KCTD5 (NP_061865), human GRASP55 (NP_056345), human Kv4.2 (AH009258), human KChIP2 (AAF33683), rat MiRP2 (NP_071571), and human SUMO1 (NP_001005781).

Acknowledgements

This work was supported by funding from the National Institutes of Health to S.A.N.G. and by funding to A. Kossiakoff for support of V.T. We thank R. Goldstein, C. R. King, A. Sullivan, and M. Toups for technical support, and A. Pandey for the constructs. Use of the APS was supported by the US Department of Energy, Office of Basic Energy Sciences (contract no. DE-AC02-06CH11357). Use of the GM/CA CAT Sector 23-IDD was funded by the National Cancer Institute (Y1-CO-1020) and General Medical Science (Y1-GM-1104).

Supplementary Data

Supplementary data associated with this article can be found, in the online version, at doi:10.1016/j.jmb.2009.01.030

References

1. Shen, N. V., Chen, X., Boyer, M. M. & Pfaffinger, P. J. (1993). Deletion analysis of K^+ channel assembly. *Neuron*, **11**, 67–76.
2. Lee, T. E., Philipson, L. H., Kuznetsov, A. & Nelson, D. J. (1994). Structural determinant for assembly of mammalian K^+ channels. *Biophys. J.* **66**, 667–673.
3. Bardwell, V. J. & Treisman, R. (1994). The POZ domain: a conserved protein–protein interaction motif. *Genes Dev.* **8**, 1664–1677.
4. Zollman, S., Godt, D., Prive, G. G., Couderc, J. & Laski, F. A. (1994). The BTB domain, found primarily in zinc finger proteins, defines an evolutionarily conserved family that includes several developmentally regulated genes in *Drosophila*. *Proc. Natl Acad. Sci.* **91**, 10717–10721.
5. Marchler-Bauer, A., Anderson, J. B., Derbyshire, M. K., DeWeese-Scott, C., Gonzales, N. R., Gwadz, M. *et al.* (2007). CDD: a conserved domain database for interactive domain family analysis. *Nucleic Acids Res.* **35**, D237–D240.
6. Abbott, G. W. & Goldstein, S. A. N. (1998). A superfamily of small potassium channel subunits: form and function of the MinK-related peptides (MiRPs). *Q. Rev. Biophys.* **31**, 357–398.
7. Stogios, P., Downs, G., Jauhal, J., Nandra, S. & Prive, G. (2005). Sequence and structural analysis of BTB domain proteins. *Genome Biol.* **6**, R82.
8. Gamse, J. T., Kuan, Y. -S., Macurak, M., Brosamle, C., Thisse, B., Thisse, C. *et al.* (2005). Directional asymmetry of the zebrafish epithalamus guides dorsoventral innervation of the midbrain target. *Development*, **132**, 4869–4881.

9. Resendes, B. L., Kuo, S. F., Robertson, N. G., Giersch, A. B. S., Honrubia, D., Ohara, O. *et al.* (2004). Isolation from cochlea of a novel human intronless gene with predominant fetal expression. *J. Assoc. Res. Otolaryngol.* **5**, 185–202.
10. Di Marcotullio, L., Ferretti, E., De Smaele, E., Argenti, B., Mincione, C., Zazzeroni, F. *et al.* (2004). REN/KCTD11 is a suppressor of Hedgehog signaling and is deleted in human medulloblastoma. *Proc. Natl Acad. Sci.* **101**, 10833–10838.
11. Zawlik, I., Zakrzewska, M., Witusik, M., Golanska, E., Kulczycka-Wojdala, D., Szybka, M. *et al.* (2006). KCTD11 expression in medulloblastoma is lower than in adult cerebellum and higher than in neural stem cells. *Cancer Genet. Cytogenet.* **170**, 24–28.
12. Van Bogaert, P., Azizieh, R., Désir, J., Aeby, A., De Meirleir, L., Florence, J. -F. *et al.* (2007). Mutation of a potassium channel-related gene in progressive myoclonic epilepsy. *Ann. Neurol.* **61**, 579–586.
13. Gandhi, T. K., Zhong, J., Mathivanan, S., Karthick, L., Chandrika, K. N., Mohan, S. S. *et al.* (2006). Analysis of the human protein interactome and comparison with yeast, worm and fly interaction datasets. *Nat. Genet.* **38**, 285–293.
14. Grigoryan, G. & Keating, A. E. (2008). Structural specificity in coiled-coil interactions. *Curr. Opin. Struct. Biol.* **18**, 477–483.
15. Bixby, K. A., Nanao, M. H., Shen, N. V., Kreusch, A., Bellamy, H., Pfaffinger, P. J. *et al.* (1999). Zn^{2+}-binding and molecular determinants of tetramerization in voltage-gated K^+ channels. *Nat. Struct. Biol.* **6**, 38–43.
16. Holm, L. & Sander, C. (1996). The FSSP database: fold classification based on structure–structure alignment of proteins. *Nucleic Acids Res.* **24**, 206–209.
17. Li, X., Romero, P., Rani, M., Dunker, A. K. & Obradovic, Z. (1999). Predicting protein disorder for N-, C-, and internal regions. *Genome Inf.* **10**, 30–40.
18. Li, X., Peng, H., Schultz, D. C., Lopez-Guisa, J. M., Rauscher, F. J., III & Marmorstein, R. (1999). Structure–function studies of the BTB/POZ transcriptional repression domain from the promyelocytic leukemia zinc finger oncoprotein. *Cancer Res.* **59**, 5275–5282.
19. Bayón, Y., Trinidad, A. G., de la Puerta, M. L., Del Carmen Rodríguez, M., Bogetz, J., Rojas, A. *et al.* (2008). KCTD5, a putative substrate adaptor for cullin3 ubiquitin ligases. *FEBS J.* **15**, 3900–3910.
20. Nanao, M. H., Zhou, W., Pfaffinger, P. J. & Choe, S. (2003). Determining the basis of channel-tetramerization specificity by X-ray crystallography and a sequence-comparison algorithm: family values (FamVal). *Proc. Natl Acad. Sci.* **100**, 8670–8675.
21. Barr, F. A., Puype, M., Vandekerckhove, J. & Warren, G. (1997). GRASP65, a protein involved in the stacking of Golgi cisternae. *Cell*, **91**, 253–262.
22. Shorter, J., Watson, R., Giannakou, M. E., Clarke, M., Warren, G. & Barr, F. A. (1999). GRASP55, a second mammalian GRASP protein involved in the stacking of Golgi cisternae in a cell-free system. *EMBO J.* **18**, 4949–4960.
23. Kim, L. A., Furst, J., Butler, M. H., Xu, S., Grigorieff, N. & Goldstein, S. A. (2004). Ito channels are octomeric complexes with four subunits of each Kv4.2 and K^+ channel-interacting protein 2. *J. Biol. Chem.* **279**, 5549–5554.
24. Kim, L. A., Furst, J., Gutierrez, D., Butler, M. H., Xu, S., Goldstein, S. A. *et al.* (2004). Three-dimensional structure of I(to); Kv4.2–KChIP2 ion channels by electron microscopy at 21 angstrom resolution. *Neuron*, **41**, 513–519.
25. Koide, A., Gilbreth, R. N., Esaki, K., Tereshko, V. & Koide, S. (2007). High-affinity single-domain binding proteins with a binary-code interface. *Proc. Natl Acad. Sci. USA*, **104**, 6632–6637.
26. Sidhu, S. S. & Kossiakoff, A. A. (2007). Exploring and designing protein function with restricted diversity. *Curr. Opin. Chem. Biol.* **11**, 347–354.
27. Weger, S., Hammer, E., Götz, A. & Heilbronn, R. (2007). Identification of a cytoplasmic interaction partner of the large regulatory proteins Rep78/Rep68 of adeno-associated virus type 2 (AAV-2). *Virology*, **362**, 192–206.
28. Van Duyne, G. D., Standaert, R. F., Karplus, P. A., Schreiber, S. L. & Clardy, J. (1993). Atomic structures of the human immunophilin FKBP-12 complexes with FK506 and rapamycin. *J. Mol. Biol.* **229**, 105–204.
29. Otwinowski, Z. & Minor, W. (1997). Processing of X-ray diffraction data collected in oscillation mode. *Methods Enzymol.* **276**, 307–326.
30. Schneider, T. R. & Sheldrick, G. M. (2002). Substructure solution with SHELXD. *Acta Crystallogr. Sect. D*, **58**, 1772–1779.
31. Terwilliger, T. C. & Berendzen, J. (1999). Automated MAD and MIR structure solution. *Acta Crystallogr. Sect. D*, **55**, 849–861.
32. Terwilliger, T. C. (2000). Maximum likelihood density modification. *Acta Crystallogr. Sect. D*, **56**, 965–972.
33. Cambillau, C. & Roussel, A. (1997). *Turbo Frodo, Version OpenGL.1.* University Aix-Marseille II, Marseille.
34. Adams, P. D., Pannu, N. S., Read, R. J. & Brunger, A. T. (1997). Cross-validated maximum likelihood enhances crystallographic simulated annealing and refinement. *Proc. Natl Acad. Sci. USA*, **94**, 5018–5023.
35. Vagin, A. A. & Teplyakov, A. (1997). An automated program for molecular replacement: MOLREP. *J. Appl. Crystallogr.* **30**, 1022–1025.
36. Murshudov, G. N., Vagin, A. A. & Dodson, E. (1997). Refinement of macromolecular structures by maximum-likelihood method. *Acta Crystallogr. Sect. D*, **53**, 240–255.
37. Collaborative Computational Project (1994). The CCP4 suit: programs for protein crystallography. *Acta Crystallogr. Sect. D*, **50**, 760–763.
38. Smart, O. S., Neduvelil, J. G., Wang, X., Wallace, B. A. & Sansom, M. S. (1996). HOLE: a program for the analysis of the pore dimensions of ion channel structural models. *J. Mol. Graphics*, **14**, 354–360.
39. Carson, M. (1996). RIBBONS. *Methods Enzymol.* **277**, 493–505.
40. Nicholls, A., Sharp, K. A. & Honig, B. (1991). Protein folding and association: insights from the interfacial and thermodynamic properties of hydrocarbons. *Proteins Struct. Funct. Genet.* **11**, 281–296.
41. Rice, P., Longden, I. & Bleasby, A. (2000). EMBOSS: The European Molecular Biology Open Software Suite. *Trends Genet.* **16**, 276–277.
42. Soh, H. & Goldstein, S. A. N. (2008). I_{SA} channel complexes include four subunits each of DPP6 and Kv4.2. *J. Biol. Chem.* **283**, 15072–15077.
43. Myszka, D. G. (1999). Improving biosensor analysis. *J. Mol. Recognit.* **12**, 279–284.
44. Clay, J. R. (2000). Determining K^+ channel activation curves from K^+ channel currents. *Eur. Biophys. J.* **29**, 555–557.